processes

MDPI

Article

Investigation of Catalytic and Photocatalytic Degradation of Methyl Orange Using Doped $LaMnO_3$ Compounds

Paula Sfirloaga [1], Madalina-Gabriela Ivanovici [1,2], Maria Poienar [1,*], Catalin Ianasi [3] and Paulina Vlazan [1]

[1] National Institute for Research and Development in Electrochemistry and Condensed Matter, 300569 Timişoara, Romania
[2] Faculty of Industrial Chemistry and Environmental Engineering, Politehnica University of Timisoara, Bv. Vasile Parvan No. 6, 300223 Timisoara, Romania
[3] "Coriolan Drăgulescu" Institute of Chemistry, Bv. Mihai Viteazul, No. 24, 300223 Timişoara, Romania
* Correspondence: maria.poienar@gmail.com

Abstract: $LaMnO_3$ and 1% Pd-, Ag-, or Y-doped perovskite type nanomaterials were prepared by the sol-gel method, followed by heat treatment at a low temperature (600 °C for 6 h). The investigation through X-ray diffraction and FT-IR spectroscopy indicated that all samples were well crystallized, without secondary phases, and that the transition metal doping changed the crystal structure from the R-3c space group for the undoped $LaMnO_3$ to the Pm-3m space group for the doped perovskite compounds. In this research paper, the efficiencies of the perovskite $LaMnO_3$ materials for methyl orange removal were analyzed, wherein the effect of the doping ions and of the pH on the catalytic activity were studied together with a kinetic approach for the $LaMnO_3$ materials at different values of the pH. Moreover, in the catalytic activity, it should be noted that a slightly better performance was obtained for the Ag-doped materials compared to the Y- and Pd-doped perovskite samples. The results presented for the perovskite $LaMnO_3$ nanomaterials reinforce the interest in these multifunctional materials to be used in industrial applications; e.g., in water treatment.

Keywords: perovskite; doping; catalysis; kinetic parameters; MO degradation

Citation: Sfirloaga, P.; Ivanovici, M.-G.; Poienar, M.; Ianasi, C.; Vlazan, P. Investigation of Catalytic and Photocatalytic Degradation of Methyl Orange Using Doped $LaMnO_3$ Compounds. *Processes* **2022**, *10*, 2688. https://doi.org/10.3390/pr10122688

Academic Editor: Alexander S. Novikov

Received: 4 November 2022
Accepted: 9 December 2022
Published: 13 December 2022

1. Introduction

In recent years, due to more pollution in the environment, intensive research has focused on effluent water treatment, as the availability of clean water is a major issue. Advanced oxidation systems have been widely studied for these applications with very good results, based on which the generated radical intermediates oxidize the organic chemicals found in wastewater [1]. In this context, scientists have been searching for promising visible-light photocatalysts compounds and, among them, perovskite ABO_3-type materials have presented interesting results [2–6].

One of the main agents causing water pollution are organic-based compounds, especially resulting from industries which have harmful effects on the environment and for human health. Perovskite-type materials have been reported to have promising results, as they can be applied for the degradation of organic pollutants [7–9]. $LaMnO_3$ has attracted particular interest, as it has been reported as a green catalyst which can be applied for the degradation of methyl orange (MO) in aqueous solution under different conditions [7,10], the degradation of other organic pollutants such as Rhodamine B (RhB) [11], and presents photocatalytic activity for the removal of methylene violet [8]. On the other hand, the doping influence of photocatalytic activity on the photodegradation of Direct Green BE was found to be higher in Ag-modified $LaMnO_3$-graphene than in pure $LaMnO_3$ and $LaMnO_3$-graphene [12]. Furthermore, Fe-substituted $LaMnO_3$ materials were investigated as heterogeneous catalysts in the H_2O_2—assisted degradation of anionic dyes (Remazol Turquoise Blue, Remazol Brilliant Yellow) and cationic dyes (methylene blue, Safranine-O)

in both the absence and presence of visible light irradiation [13]. Recently, the sustainable removal of 17α-ethynylestradiol (EE2) from aqueous environment has been shown using rare-earth-doped $LaMnO_3$ nanomaterials in [14], and the best removal efficiency was reached in the presence of Ho in $LaMnO_3$, when 77% of endocrine disruptors EE2 were degraded after 30 min of UV irradiation.

In order to provide more insight on and find new candidates for semiconductor photocatalysts, the organic pollutant degradation activity of undoped and 1% Pd-, Ag-, or Y-doped $LaMnO_3$ perovskite materials is investigated and presented in this study; in the case of 1% Pd-, Ag- or Y-doped perovskite compounds, for the first time. Furthermore, a kinetic study was employed for the degradation of MO over the undoped $LaMnO_3$ in dark conditions in the 2−4 pH range, and, to the best of our knowledge, no kinetics have been reported in the scientific literature for the catalytic activity of $LaMnO_3$ to degrade MO. Our results show that these materials with a perovskite-type structure could be considered as viable solar-driven photocatalysts due to their efficiency for MO removal under solar irradiation. The 1% Pd, Ag, or Y doping affects the perovskite crystal structure, and the materials showed catalytic or photocatalytic activity in the acidic medium. A slightly better performance for MO degradation under dark conditions is registered for the Ag-doped $LaMnO_3$ samples compared to the Y- and Pd-doped $LaMnO_3$ materials.

2. Materials and Method

Pristine $LaMnO_3$ and 1% Pd-, Ag-, or Y-doped samples were prepared using the sol-gel method, followed by heat treatment at a low temperature (600 °C for 6 h). The following reagents were used for the synthesis of the studied materials: $La(NO_3)_3 \cdot 6H_2O$, $Mn(NO_3)_2 \cdot 4H_2O$ and 2M NaOH solution, used as starting materials. To study the influence of doping on the catalytic and photocatalytic properties of perovskite-type $LaMnO_3$ materials, the $LaMnO_3$ compounds were doped with 1% Pd, Ag, or Y by adding the following reactants: $Pd(NO_3)_2 \cdot 2H_2O$, $AgNO_3$, and $Y(NO_3) \cdot 6H_2O$. All chemicals were analytical grade from Sigma-Aldrich, and were used as received without any further purification.

The abovementioned precursors were dissolved in water, alcohol mixture, and then, in order to homogenize the mixture, it was stirred at room temperature for 30 min followed by the addition of citric acid under continuous stirring, while the temperature was raised and kept at 140 °C until the gels were obtained. The resulting gels were dried in an oven at 80 °C for 4 h and then calcined at 600 °C for 6 h to obtain the final perovskite samples. Perovskite manganite synthesis by sol-gel technique has been previously reported for undoped [15–23], doped (for example with Fe [24], N [16], Ag [25], or Sr [21]), or substituted $LaMnO_3$ materials (with Pd [26], Ca [15], Fe, Co, or Ni [23]), and is considered to be a successful and flexible synthesis route to obtain well-crystallized micro- or nanomaterials from this family of compounds [27].

Room temperature (RT) X-ray powder diffraction (XRD) data were collected using a PANalytical X'Pert PRO MPD diffractometer with Cu-Kα radiation (λ = 1.5418 Å) in the 2θ = 10–80° range. For FT-IR analysis, a Shimadzu Prestige FT-IR spectrometer was used in the 400–4000 cm^{-1} range using KBr pellets. The morphology of the investigated samples was studied using scanning electron microscopy (SEM) (Inspect S) equipped with an energy dispersive X-ray (EDX).

Investigation of the catalytic and photocatalytic properties of the pristine and doped $LaMnO_3$ with transition metals, Pd, Ag, or Y, were carried out by monitoring the degradation capacity of MO in aqueous solutions considering different experimental conditions, which were selected based on factors that known in the literature to affect catalytic and photocatalytic behavior. Therefore, two aspects were considered for this study: evaluation of the pH effect on the $LaMnO_3$ catalytic activity (selected in the range between 2 and 5) and evaluation of the doping in the perovskite structure on the photocatalytic activity. The pH was modified using small volumes of 0.1M HNO_3 (65% reagent Ph. Eur., Sigma Aldrich) solution from the pH = 5 (for the initial concentration of MO aqueous solution) to pH = 4, 3 and 2. A volume of 40 mL MO (reagent Ph Eur.) aqueous solution of 12 ppm initial concentration was used for all experiments. The catalyst (of 120 ppm concentration)

was added to a glass container together with the solution and was magnetically stirred for 90 min. In order to determine MO degradation over time, the absorbance of the MO solution was monitored every 10 min using a UV-VIS spectrometer (portable Jaz spectrometer from Ocean Optics). For this, 2–3 mL of the mixed solution (catalyst with MO aqueous solution) was separated by centrifugation and the solution was then inserted into the UV-VIS cuvette. The experimental set-up used for the absorbance measurements was as described in a previous study [28]. The degradation rate of MO (%) was calculated with Equation (1):

$$Degradation\ rate(\%) = \frac{(A_0 - A_t)}{A_0} \cdot 100 \quad (1)$$

where A_0—the absorbance of the MO aqueous solution in the moment of catalyst addition (time t = 0), A_t—the absorbance of the MO solution at time t.

The catalytic experiments were performed at room temperature in dark conditions, whereas the photocatalytic experiments were performed under simulated solar radiation (provided by Sol2A 94042A, Oriel Instruments/Newport Corporation). The visible and respective UV irradiance at the surface of the mixed solution was 957 W/m^2 and 1.02 mW/cm^2, respectively. Moreover, a kinetic approach was employed for the undoped perovskite $LaMnO_3$ materials in order to determine the reaction rate of catalytic MO degradation over $LaMnO_3$ when the solution pH was changed from 2 to 5.

3. Results and Discussion

3.1. XRD Analysis

Analysis by X-ray diffraction was performed for the samples obtained as described in the previous section. The sol-gel method with thermal treatment at a low temperature obtains well-crystallized samples without secondary phases (Figure 1), as has been already reported in previous studies for undoped and doped/substituted $LaMnO_3$ perovskite samples [15–17,24–26]. The diffractogram visualizations in Figure 1 indicate that some of the peaks are split for the undoped material compared to the 1% Pd^{2+}, Ag^{+}, or Y^{3+} doped $LaMnO_3$ samples (insert Figure 1). The $LaMnO_3$ compound obtained using the sol-gel method is indexed in the R-3 c space group [JCPDS card file no. 01-089-0678] and, for the doped materials, the Pm-3m space group is used [JCPDS card file no. 01-075-0440], as well as for the rare-earth-doped $LaMnO_3$ materials in [14]. Therefore, upon doping in the $LaMnO_3$ samples with Pd, Ag, or Y (this study), with rare earth Eu, Tb, and Ho [14], Pr or Eu [29], Na or Ca ion [30] changes are induced within the perovskite structure, which could have a great effect on the properties of the obtained materials.

3.2. FT-IR Analysis

Figure 2 shows the FT-IR spectra for pristine $LaMnO_3$ and 1% Pd-, Ag-, or Y-doped $LaMnO_3$ samples recorded in the 400–4000 cm^{-1} spectral range. It is observed that several absorption bands at 433, 619, 630, 853, 1373, 1477, 1637, 2924, and 3437 cm^{-1} are registered for these samples. The significant absorption bands for the $LaMnO_3$ materials from this work are approximately located in the same spectral range as the perovskite $LaMnO_3$ materials from the previous study obtained using the sol-gel synthesis method [14,17,31].

Two transmission bands around 620 and 430 cm^{-1} are observed for the materials; the band around 430 cm^{-1} directly corresponds to the bending mode (ν_b), owing to the change in the Mn–O–Mn bond angle. The frequency band around 620 cm^{-1} is related to the stretching mode (ν_s) of Mn–O or Mn–O–Mn bonds, which embraces the change in the bond length of Mn–O because of the internal motion [32]. These two bands are interrelated to the neighborhoods surrounding the MnO_6 octahedral in the ABO_3 perovskite and confirm the formation of a perovskite structure [33].

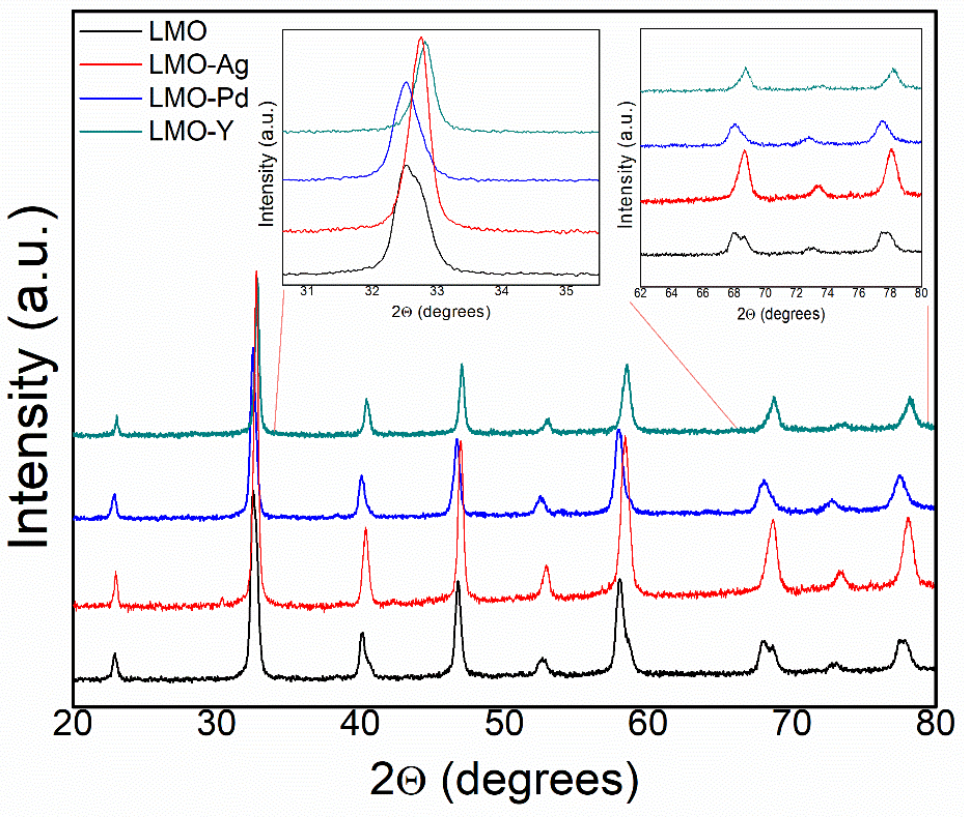

Figure 1. XRD patterns for the undoped and 1% Pd-, Ag-, or Y-doped $LaMnO_3$ perovskite materials. Insert: Zoom of the XRD patterns in the 2θ = 30.5–35.5° and 2θ = 62–80° regions.

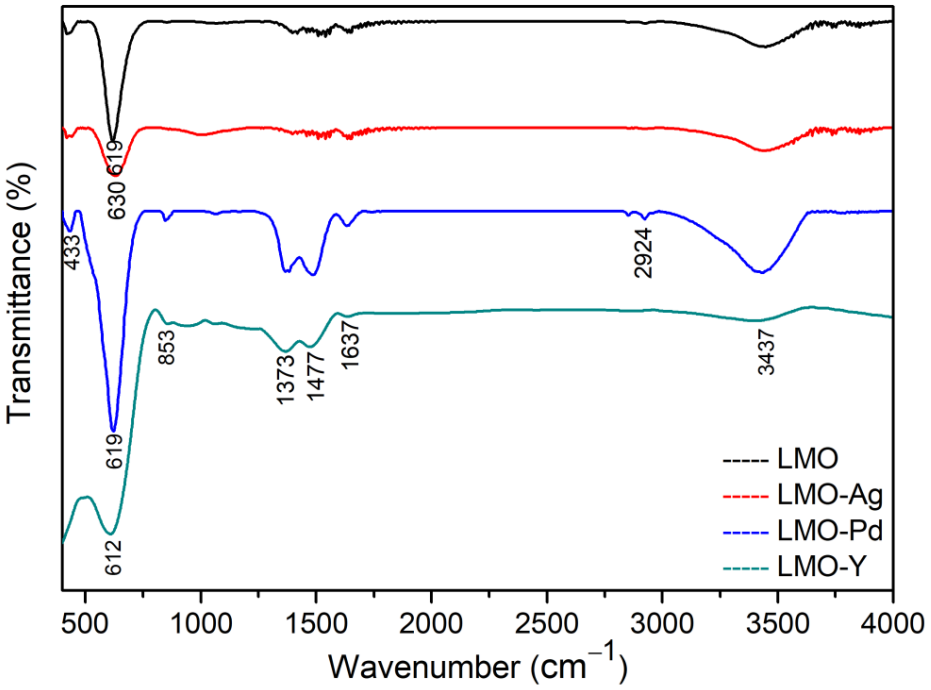

Figure 2. FT-IR spectra of undoped $LaMnO_3$ and 1% Pd-, Ag-, or Y-doped $LaMnO_3$ materials.

In the FT-IR spectra for the Pd-doped $LaMnO_3$ and Y-doped $LaMnO_3$ samples, some additional peaks at 853, 1373, 1477, 1637, and 2924 cm^{-1} appear. The low intensity peak located at 857 cm^{-1}, which appears only in doped samples, could be attributed to the Me-O

bond (Me = Pd, Y). The two bands located at 1477 and 1373 cm^{-1} can be attributed to the δOH and γOH vibrational modes of H_2O molecules [34].

The 2500–3600 cm^{-1} region encloses stretching O–H modes (strong and wide depending on the environment), stretching C–H modes (generally strong), and stretching N–H modes typical in amine groups [35]. As in the synthesis process, no organic compounds were used, the 2924 cm^{-1} peak could be attributed to the O-H group from the water in the environment.

The broad bands of low intensity with the maximum around 3437 and 1637 cm^{-1} can be assigned to O-H stretching modes of surface-adsorbed water, due to the contact of the sample with the environment. These stretching vibrations of weakly-bound water interact with its environment via hydrogen bonding [36].

3.3. SEM-EDX/ Element Mapping

Figure 3 shows the SEM micrograph of undoped and doped $LaMnO_3$ materials. In the case of the undoped and Pd-doped $LaMnO_3$, the surface morphology shows that the particles are agglomerated into asymmetric formations, although these agglomerations are composed of extremely fine particles. The EDX mapping for the $LaMnO_3$ compound has also been reported in [14], where the uniform distribution of elements was also confirmed.

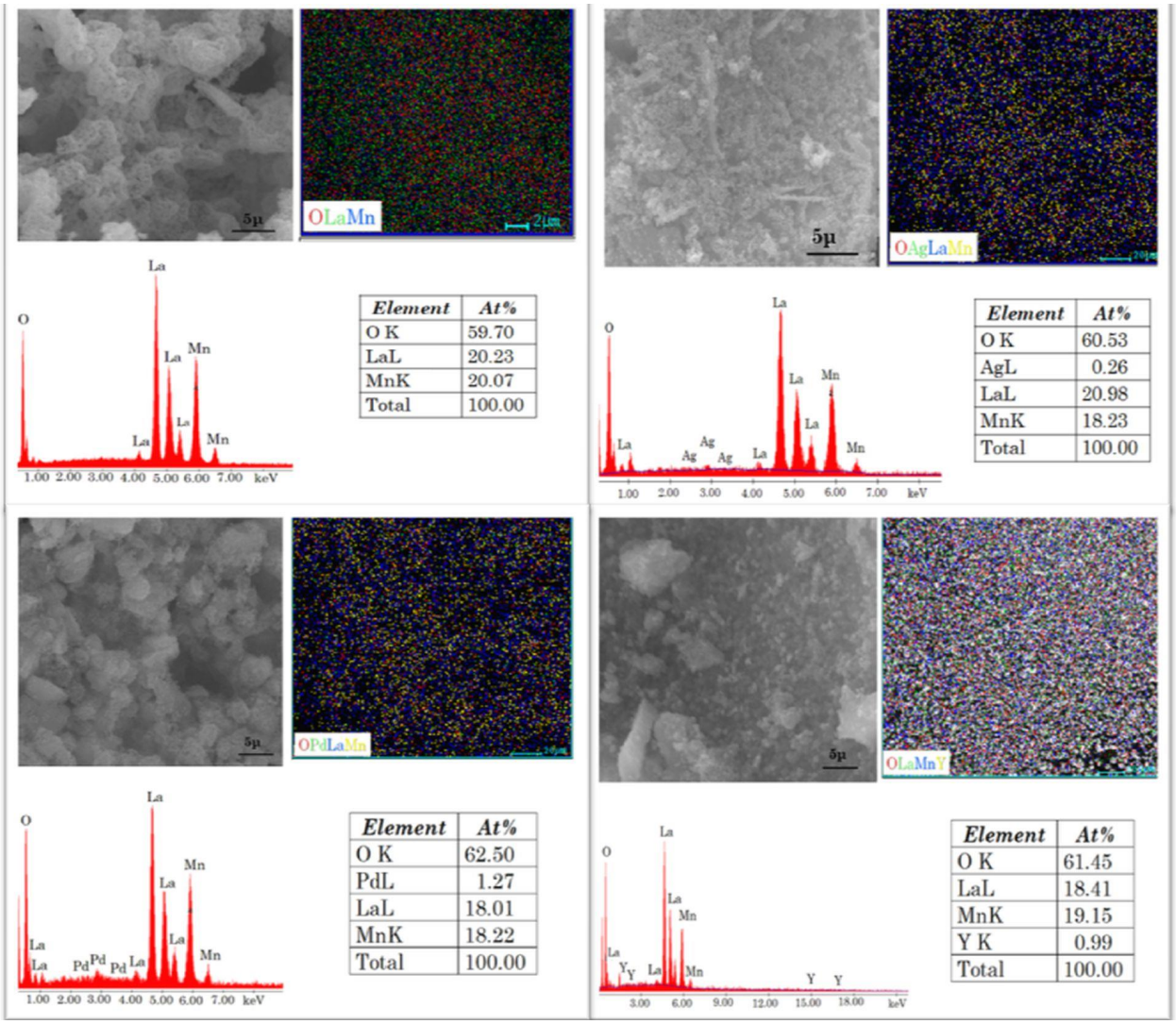

Figure 3. SEM images, element mapping, EDX spectrum, and quantification of undoped, Ag-, Pd-, and Y-doped $LaMnO_3$ materials.

The qualitative analysis of Ag- or Y-doped lanthanum manganite exhibit spherically aggregated particles free from agglomeration. The EDX spectra show, in addition to the purity of the obtained materials, the presence of the three dopants. Thus, quantification of the elements confirms that the expected level of doping is present in each sample, maintaining the stoichiometry of the compound. Moreover, elements mapping highlighted the uniform distribution of the component elements for each material (Figure 3).

3.4. Catalytic Activity of the $LaMnO_3$ Nanomaterials

3.4.1. The Effect of the pH on the MO Absorption and on the Catalytic MO Degradation over Undoped LMO; Kinetic Parameters Determination

As a first step toward the evaluation of the catalytic properties of the $LaMnO_3$ compound, the change in the visible absorption for the MO aqueous solution was investigated (Figure 4). The maximum absorption of the initially prepared solution of 12 ppm concentration (pH = 5) was registered at a wavelength of 467 nm. The increase in the solution acidity led to a shift of the absorbance band toward a higher wavelength (505 nm) and also to an increase of the band intensity from 0.92 (at pH = 5) to 1.29 (at pH = 4), 1.39 (at pH = 3), and 1.52 (at pH = 2). Visually, the bathochromic shift was observed by the color change from yellow-orange to orange-red nuances (as visualized in Figure 4 down). As reported in the literature, the redshift is obtained as a result of chromophoric group (NN bond) protonation of MO in the acidic medium, as the acidic structures absorbs light in the spectrum of the red-green domain [37,38]. Furthermore, the pH affects the surface charge of the $LaMnO_3$ and the adsorption of the species on the material surface, determining the catalytic activity for MO degradation [9,39].

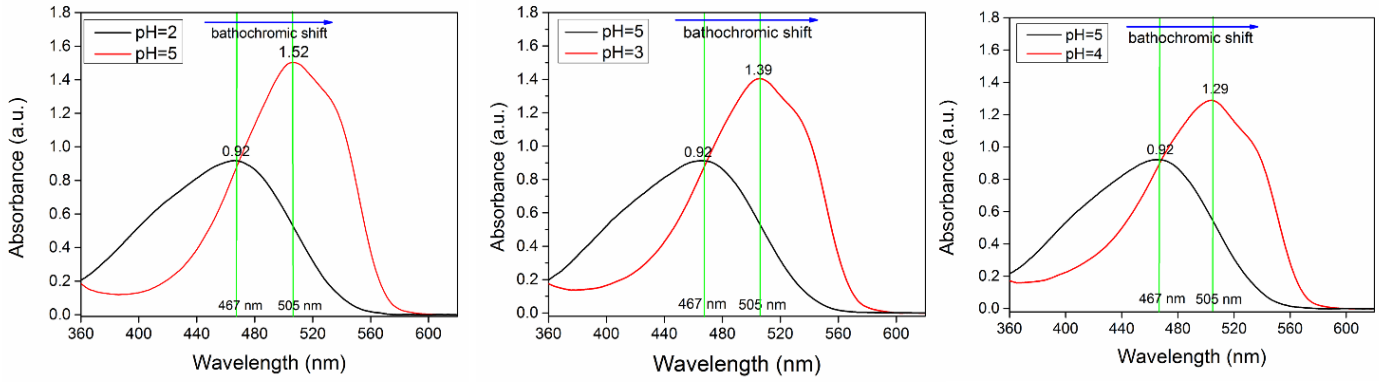

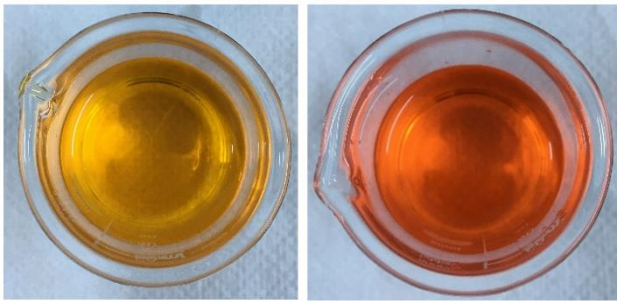

Figure 4. Bathochromic shift of the MO solutions absorbance band caused by the increase of the aqueous solution acidity (**up**). Color of the MO aqueous solution before (**left**) and after (**right**) the addition of small volumes of HNO_3 (0.1M) (**down**).

As represented in Figure 5, the removal of MO from the aqueous solution under dark conditions increased as the pH values decreased from 5 to 2. At pH = 2, the maximum removal of MO (97%) was achieved after 50 min of reaction, whereas at pH = 3, the maximum removal of MO (96%) was reached after 80 min. No degradation occurred at

pH = 5, but, at pH = 4, 83% of MO from the aqueous was degraded after 90 min of reaction. The kinetics of the catalytic reactions carried out at pH = 2, 3, and 4 were studied based on the kinetics models of zero-, first-, and second-order reactions. The integrated forms of kinetics equations are:

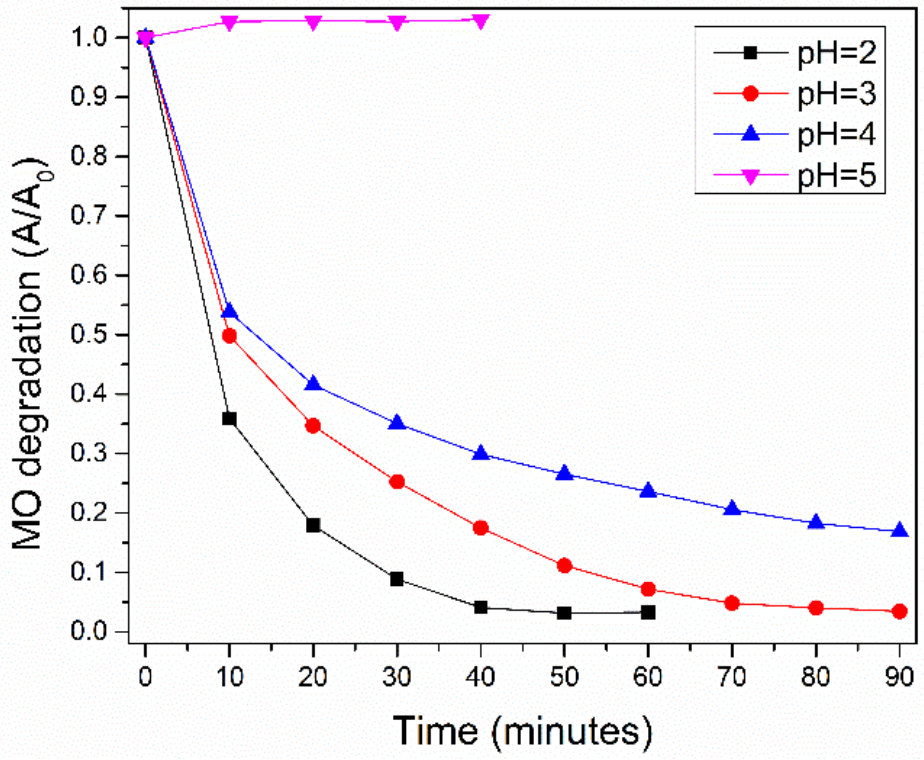

Figure 5. Catalytic degradation of MO (40 mL of 12 ppm initial concentration) by $LaMnO_3$ (120 ppm concentration) in the pH range values of 2–5.

Zero-order reaction kinetics

$$C_t = C_0 - k_0 t \quad (2)$$

First-order reaction kinetics

$$C_t = C_0 e^{-k_1 t} \quad (3)$$

Second-order reaction kinetics

$$\frac{1}{C_t} = \frac{1}{C_0} + k_2 t \quad (4)$$

where C_t—concentration of reactant at time t, C_0—concentration of reactant at initial time, and k_0, k_1, and k_2—rate constant for zero-, first-, and second-order reactions.

The constant rate of MO degradation by $LaMnO_3$ materials carried out in the pH range of 2–4 was determined by plotting ln (C_t/C_0), $C_t - C_0$, and $1/C_t - 1/C_0$ versus time [40–42]. The concentration at time (t) was calculated considering the MO degradation rate and the known initial concentration of the solution. Therefore, the fitting parameters (regression coefficient—R^2 and rate constant—k) results for MO degradation at different pH values are presented in Table 1. Based on the calculated regression coefficient, the degradation of MO catalyzed by the $LaMnO_3$ can be attributed to the pseudo-first- and pseudo-second-order reaction for pH = 2, pH = 3, and pH = 4 with corresponding pseudo-constant rates of 0.07 min^{-1}, 0.04 min^{-1}, and 0.01 L mg^{-1} min^{-1}, respectively [43].

Table 1. Fitting parameters calculated for catalytic degradation reaction of MO obtained at different pH values (2, 3, and 4).

Fitting Parameters (for Zero, First and Second Order Reaction)		Reaction 1	Reaction 2	Reaction 3
		pH = 2	pH = 3	pH = 4
zero order reaction	k_0 (mg L^{-1} min^{-1})	0.20	0.10	0.08
	R^2	0.72	0.72	0.67
first order reaction	k_1 (min^{-1})	0.07	0.04	0.02
	R^2	0.98	0.98	0.91
second order reaction	k_2 (L mg^{-1} min^{-1})	0.05	0.03	0.01
	R^2	0.91	0.914	0.99

3.4.2. The Dopant Effect on the Catalytic and Photocatalytic Properties of $LaMnO_3$—Comparative Approach

Furthermore, the photocatalytic properties of undoped and 1% Pd-, Ag-, or Y-doped $LaMnO_3$ were studied in order to investigate the impact of transition metals doping in the $LaMnO_3$ perovskite structure (Figure 6). The reaction of MO degradation was carried out in acidic medium, and the solution pH was settled to 4 so the experimental conditions were less severe, involving minimal changes of the medium for the reaction to occur.

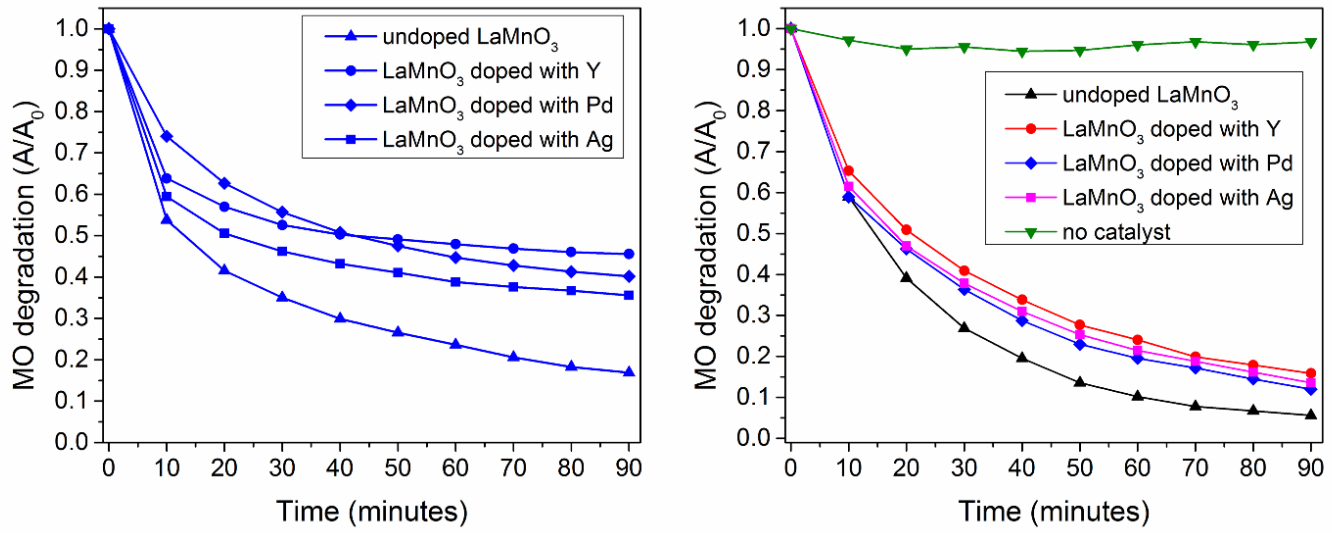

Figure 6. Degradation of MO from aqueous solution (40 mL of 12 ppm initial concentration) by 1% Pd-, Ag-, or Y-doped and undoped $LaMnO_3$ (120 ppm catalyst concentration) in acidic medium (pH = 4) under dark (**left**) and artificial solar light (**right**).

When compared to $LaMnO_3$, the degradation rates obtained for Y-, Pd-, and Ag-doped $LaMnO_3$ decreased by 54.63%, 60.31%, and 64.56% after 90 min of reaction. Under artificial solar irradiation, the degradation rate reached 94.7% for the undoped $LaMnO_3$, with close values (84.5%, 88%, and 86%) for $LaMnO_3$ doped with Y, Pd, and Ag, from which 4.65% of MO was degraded by photolysis. The improved efficiency of MO removal under solar irradiation indicates that Y-, Pd-, or Ag-doped $LaMnO_3$ can be considered as solar light active photocatalysts, validating the multifunctional behavior of the perovskites as catalysts. Our findings indicate that the dopants did not improve, nor the catalytic either the photocatalytic properties extensively studied for $LaMnO_3$, but, notably, the Ag doping led to a better performance for MO degradation under dark conditions when compared to Y and Pd, whereas Pd-, Ag-, or Y-doped $LaMnO_3$ showed similar performances as photocatalysts. The MO degradation was induced by the well-known superior oxidation catalytic activity of the perovskites, as has already been reported in [44]. In the ABO_3-type perovskite structure, the A cation is the larger in size and is 12-fold coordinated with oxygen

anions, while the B cation is 6-fold coordinated with oxygen anions. From the catalytic activity perspective, the A cations are generally catalytically inactive, while the B cations are responsible for the catalytic response of the ABO_3, so that B ions are situated at a relatively large distance (ca. 0.4 nm) away from each other, allowing, in this way, a reactant molecule to interact with a single site. Doping the A and B sites is a common practice by which to modify the catalytic response of the perovskites by altering the crystal structure and disturbing the oxidation states of the cations [3,5,12,34]. The structural changes followed the dopant incorporation into the perovskite lattice, depending on the ionic radius of the dopant; thus, in this study, the ionic radii are: Ag^+ (1.15 Å), Pd^{2+} (0.86 Å), Y^{3+}(0.9 Å).

Moreover, a blueshift of the MO absorbance appeared in the photocatalytic reaction (Figure 7), which can be explained by the agglomeration of MO molecules in the aqueous solution as the dye dilution increases, indicative of degradation instead of exclusive adsorption [10,11]. From the point of view of the mechanistic aspect of catalytic and photocatalytic reactions, the reaction occurs as a result of adsorption of the reactant on the catalyst surface, followed by the catalyzed reaction [7,45]. MO degradation is favored in acidic medium, as the pH changes leads to changes in MO adsorption on the catalyst surface and in the photodegradation mechanism. MO is an anionic dye and its adsorption is facilitated in acidic medium and, in addition, it has been reported to be less stable and prone to degradation [46,47]. In dark conditions, the degradation of MO can be explained by the interaction between MO and the catalyst surface, resulting in the degradation of azo bonds of MO and the generation of electrons. Following sequential reactions, the electrons lead to the formation of hydroxyl radicals. Under illumination, the pairs of electrons and holes are formed and lead to the formation of hydroxyl radicals. Therefore, hydroxyl radicals are the main oxidative species responsible for MO degradation, both in dark condition and under illumination [46–50]:

$$OH + MO \rightarrow \text{ intermediates } \rightarrow SO_4^{2-} + NO_3^- + NH_4 + CO_2 + H_2O \quad (5)$$

Table 2 presents the results obtained in others studies related to catalytic MO degradation over $LaMnO_3$ and other types of perovskites carried out in dark conditions or under irradiation (UV, light, or solar radiation). As an example, MO degradation is higher (83%) after 90 min of reaction at pH = 4 and in dark conditions; in this work, when compared with study [10], the degradation of MO is 73% at pH = 3.6. Similar MO degradation efficiencies are obtained in both this work and study [22], under illumination. By summarizing multiple studies regarding the catalytic and photocatalytic properties of perovskites for MO degradation, we consider that this work comes with relevant novelty in terms of the scientific literature by studying the effect of transitional dopants, and of the pH on the photodegradation of MO and on the assisted dark catalysis.

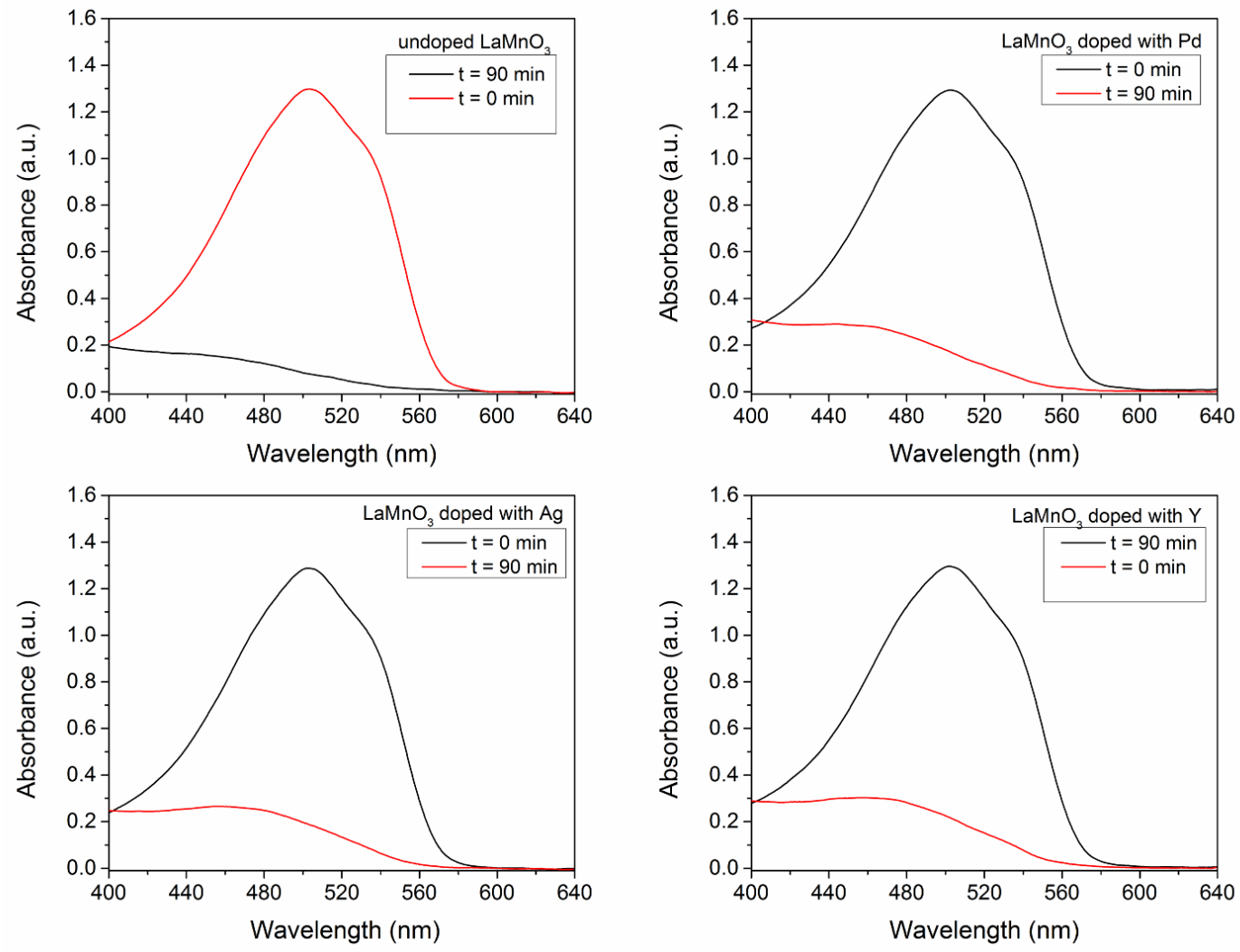

Figure 7. Blueshift of MO absorbance peak in the photodegradation process by undoped and 1% Pd-, Ag-, and Y-doped $LaMnO_3$.

Table 2. Scientific literature review of MO catalytic degradation over various types of perovskites.

Perovskite Type	Catalyst Concentration (ppm)	Aqueous Solution Volume (mL)	MO Concentration (ppm)	pH	MO Degradation Percent [%]	Dark or Illumination	Source
$LaMnO_3$	200	50	3	-	90% after 60 min	Visible light	[7]
$LaMnO_3$	60	40	6	2	98% after 90 min	Visible light	[22]
$LaMnO_3$	500	100	20	-	~57% after 90 min	Visible light	[51]
$LaMnO_3$	500	20	6.5	2.6	~90% in 90 min	dark	[10]
$LaMnO_3$	500	20	6.5	3.3	~87% in 90 min	dark	[10]
$LaMnO_3$	500	20	6.5	3.6	~73% in 90 min	dark	[10]
$LaMnO_3$	500	20	6.5	3.1	~100% in 60 min	solar	[10]
$LaNiO_3$	1500	100	5	-	94.3% in 4 h	dark	[52]
$La_{0.5}Sr_{0.5}CoO_3$	25	100	20	2.5	99.5% in 25 min	dark	[49]
$La_{0.5}Sr_{0.5}CoO_3$	25	100	20	2.5	99.7% in 25 min	UV radiation	[49]
$LaMnO_3$	120	40	12	4	83% in 90 min	dark	This work
$LaMnO_3$	120	40	12	4	94.7% in 90 min	Solar radiation	This work

4. Conclusions

Undoped and 1% Pd-, Ag-, or Y-doped $LaMnO_3$ perovskite materials obtained by the sol-gel method, followed by heat treatment at a low temperature (600 °C for 6 h), were

studied in this research for the catalytic and photocatalytic degradation of methyl orange. The X-Ray diffraction patterns are characteristic of a perovskite structure with a different symmetry induced by doping (Pm-3m compared to R-3c for undoped $LaMnO_3$). The catalytic activity of $LaMnO_3$ was investigated for the removal of MO from the aqueous solution under dark conditions, and it was observed that it increased as the pH values decreased from 5 to 2; at pH = 2, the maximum removal of MO (97%) was achieved after 50 min of reaction, whereas at pH = 3, the maximum removal of MO (96%) was reached after 80 min; at pH = 4, 83% of MO from the aqueous was degraded after 90 min of reaction, while no degradation occurred at pH = 5. Moreover, the kinetics of catalytic reactions carried out for the different values of the pH were studied based on the kinetics model of zero-, first-, and second-order reactions.

When compared to $LaMnO_3$, the degradation rates obtained for Y-, Pd-, or Ag-doped $LaMnO_3$ decreased by 54.63%, 60.31%, and 64.56% after 90 min of reaction. Under artificial solar irradiation, the degradation rate reached 94.7% for the undoped $LaMnO_3$ and close values (84.5%, 88%, and 86%) were obtained for Y-, Pd-, or Ag-doped $LaMnO_3$ samples. On the other hand, the Ag-doped $LaMnO_3$ led to better performance for MO degradation under dark conditions when compared to Y and Pd, which was probably related to some structural features facilitating this slight enhancement of properties.

Author Contributions: Conceptualization, P.S. and M.P.; methodology, P.S. and M.-G.I.; validation, P.S., M.P. and M.-G.I.; formal analysis, P.V., C.I., M.P., M.-G.I. and P.S.; investigation, P.V., M.P., M.-G.I. and P.S.; data curation, M.P. and M.-G.I.; writing—original draft preparation, P.V., M.P., M.-G.I. and P.S.; writing—review and editing, P.V., C.I., M.P., M.-G.I. and P.S.; supervision, P.S.; project administration, P.S.; funding acquisition, P.S., P.V. and M.P. All authors have read and agreed to the published version of the manuscript.

Funding: This work was supported by the Experimental Demonstrative Project 683PED/21/06/2022.

Data Availability Statement: The data that support the findings of this study are available from the authors, upon reasonable request.

Acknowledgments: Financial support for this work was provided by the Experimental Demonstrative Project 683PED/21/06/2022.

Conflicts of Interest: The authors have no relevant financial or non-financial interests to disclose.

References

1. Rojas-Cervantes, M.L.; Castillejos, E. Perovskites as Catalysts in Advanced Oxidation Processes for Wastewater Treatment. *Catalyst* **2019**, *9*, 230. [CrossRef]
2. Hu, J.; Men, J.; Ma, J.; Huang, H. Preparation of $LaMnO_3$/graphene thin films and their photocatalytic activity. *J. Rare Earths* **2014**, *32*, 1126–1134. [CrossRef]
3. Hu, J.; Liu, Y.; Men, J.; Zhang, L.; Huang, H. Ag modified $LaMnO_3$ nanorods-reduced graphene oxide composite applied in the photocatalytic discoloration of direct green. *Solid State Sci.* **2016**, *61*, 239–245. [CrossRef]
4. Gao, P.; Li, N.; Wang, A.; Wang, X.; Zhang, T. Perovskite $LaMnO_3$ hollow nanospheres: The synthesis and the application in catalytic wet air oxidation of phenol. *Mater. Lett.* **2013**, *92*, 173–176. [CrossRef]
5. Andrei, F.; Zavoianu, R.; Marcu, I.C. Complex Catalytic Materials Based on the Perovskite-Type Structure for Energy and Environmental Applications. *Materials* **2020**, *13*, 5555. [CrossRef]
6. Labhasetwar, N.; Saravanan, G.; Megarajan, S.K.; Manwar, N.; Khobragade, R.; Doggali, P.; Grasset, F. Perovskite-type catalytic materials for environmental applications. *Sci. Technol. Adv. Mater.* **2015**, *16*, 036002. [CrossRef]
7. Dhinesh Kumar, R.; Thangappan, R.; Jayavel, R. Enhanced visible light photocatalytic activity of $LaMnO_3$ nanostructures for water purification. *Res. Chem. Intermed.* **2018**, *44*, 4323–4337. [CrossRef]
8. Priyatharshni, S.; Kumar, S.R.; Viswanathan, C.; Ponpandian, N. Morphologically tuned $LaMnO_3$ as an efficient nanocatalyst for the removal of organic dye from aqueous solution under sunlight. *J. Environ. Chem. Eng.* **2020**, *8*, 104146. [CrossRef]
9. Tran, T.H.; Phi, T.H.; Nguyen, H.N.; Pham, N.H.; Nguyen, C.V.; Ho, K.H.; Doan, Q.K.; Le, V.Q.; Nguyen, T.T.; Nguyen, V.T. Sr doped $LaMnO_3$ nanoparticles prepared by microwave combustion method: A recyclable visible light photocatalyst. *Results Phys.* **2020**, *19*, 103417. [CrossRef]
10. Rekavandi, N.; Malekzadeh, A.; Ghiasi, E. Methyl orange degradation using nano-$LaMnO_3$ as a green catalyst under the mild conditions. *Nanochem. Res.* **2019**, *4*, 1–10.

11. Dhiman, T.K.; Singh, S. Enhanced catalytic and photocatalytic degradation of organic pollutans Rhodamine -B by $LaMnO_3$ nanoparticles synthesized by non -aqueous sol-gel route. *Phys. Status Solidi* **2019**, *216*, 1900012. [CrossRef]
12. Hu, J.; Men, J.; Liu, Y.; Huang, H.; Jiao, T. One-pot synthesis of Ag-modified $LaMnO_3$-graphene hybrid photocatalysts and application in the photocatalytic discoloration of an azo-dye. *RSC Adv.* **2015**, *5*, 54028–54036. [CrossRef]
13. Jauhar, S.; Dhiman, M.; Bansal, S.; Singhal, S. Mn^{3+} ion in perovskite lattice: A potential Fenton's reagent exhibiting remarkably enhanced degradation of cationic and anionic dyes. *J. Sol-Gel Sci. Technol.* **2015**, *75*, 124–133. [CrossRef]
14. Šojić Merkulov, D.; Vlazan, P.; Poienar, M.; Bognár, S.; Ianasi, C.; Sfirloaga, P. Sustainable removal of 17α-ethynylestradiol from aqueous environment using rare earth doped lanthanum manganite nanomaterials. *Catal. Today* **2022**. [CrossRef]
15. Sfirloaga, P.; Poienar, M.; Malaescu, I.; Lungu, A.; Mihali, C.V.; Vlazan, P. Electrical conductivity of Ca-substituted lanthanum manganites. *Ceram. Int.* **2018**, *44*, 5823–5828. [CrossRef]
16. Sfirloaga, P.; Sebarchievici, I.; Taranu, B.; Poienar, M.; Vlase, G.; Vlase, T.; Vlazan, P. Investigation of physico-chemical features of lanthanum manganite with nitrogen addition. *J. Alloys Compd.* **2020**, *843*, 155854. [CrossRef]
17. Sfirloaga, P.; Poienar, M.; Malaescu, I.; Lungu, A.; Vlazan, P. Perovskite type lanthanum manganite: Morpho-structural analysis and electrical investigations. *J. Rare Earths* **2018**, *36*, 499–504. [CrossRef]
18. El-Moez, A.; Mohamed, A.; Alvarez-Alonso, P.; Hernando, B. The intrinsic exchange bias effect in the $LaMnO_3$ and $LaFeO_3$ compounds. *J. Alloys. Compd.* **2021**, *850*, 156713. [CrossRef]
19. Elsiddig, Z.A.; Xu, H.; Wang, D.; Zhang, W.; Guo, X.; Zhang, Y.; Sun, Z.; Chen, J. Modulating Mn^{4+} Ions and Oxygen Vacancies in Nonstoichiometric $LaMnO_3$ Perovskite by a Facile Sol-Gel Method as High-Performance Supercapacitor Electrodes. *Electrochim. Acta* **2017**, *253*, 422–429. [CrossRef]
20. Li, Y.; Xue, L.; Fan, L.; Yan, Y. The effect of citric acid to metal nitrates molar ratio on sol–gel combustion synthesis of nanocrystalline $LaMnO_3$ powders. *J. Alloys Compd.* **2009**, *478*, 493–497. [CrossRef]
21. Onrubia, J.A.; Pereda-Ayo, B.; De-La-Torre, U.; González-Velasco, J.R. Key factors in Sr-doped $LaBO_3$ (B = Co or Mn) perovskites for NO oxidation in efficient diesel exhaust purification. *Appl. Catal. B Environ.* **2017**, *213*, 198–210. [CrossRef]
22. Shaterian, M.; Enhessari, M.; h Rabbani, D.; Asghari, M.; Salavati-Niasari, M. Synthesis, Characterization and Photocatalytic Activity of $LaMnO_3$ Nanoparticles. *Appl. Surf. Sci.* **2014**, *318*, 213–217. [CrossRef]
23. Yin, X.; Wang, S.; Wang, B.; Shen, L. Perovskite-type $LaMn_{1-x}B_xO_{3+\delta}$ (B = Fe, Co and Ni) as oxygen carriers for chemical looping steam methane reforming. *Chem. Eng. J.* **2021**, *422*, 128751. [CrossRef]
24. Sfirloaga, P.; Malaescu, I.; Marin, C.N.; Poienar, M.; Vlazan, P. Effect of Fe-Doping on the Structural, Morphological and Electrical Properties of $LaMnO_3$. *AIP Conf. Proc.* **2020**, *2218*, 040003.
25. Sfirloaga, P.; Vlase, G.; Vlase, T.; Malaescu, I.; Marin, C.N.; Vlazan, P. Silver doping in lanthanum manganite materials: Structural and electrical properties. *J. Therm. Anal. Calorim.* **2020**, *142*, 1817–1823. [CrossRef]
26. Sfirloaga, P.; Malaescu, I.; Marin, C.N.; Vlazan, P. The effect of partial substitution of Pd in $LaMnO_3$ polycrystalline materials synthesized by sol–gel technique on the electrical performance. *J. Sol-Gel Sci. Technol.* **2019**, *92*, 537–545. [CrossRef]
27. Navas, D.; Fuentes, S.; Castro-Alvarez, A.; Chavez-Angel, E. Review on Sol-Gel Synthesis of Perovskite and Oxide Nanomaterials. *Gels* **2021**, *7*, 275. [CrossRef]
28. Taranu, B.O.; Ivanovici, M.-G.; Svera, P.; Vlazan, P.; Sfirloaga, P.; Poienar, M. $Ni_{11}(HPO_3)_8(OH)_6$ multifunctional materials: Electrodes for oxygen evolution reaction and potential visible-light active photocatalysts. *J. Alloys Compd.* **2020**, *848*, 156595. [CrossRef]
29. Najjar, H.; Bâtis, H.; Lamonier, J.-F.; Mentré, O.; Giraudon, J.-M. Effect of praseodymium and europium doping in $La_{1-x}Ln_xMnO_{3+\delta}$ (Ln: Pr or Eu, $0 \leq x \leq 1$) perovskite catalysts for total methane oxidation. *Appl. Catal. A: Gen.* **2014**, *469*, 98–107. [CrossRef]
30. Malavasi, L.; Ritter, C.; Mozzati, M.C.; Tealdi, C.; Saiful Islam, M.; Azzoni, C.B.; Flor, G. Effects of cation vacancy distribution in doped $LaMnO_{3+\delta}$ perovskites. *J. Solid State Chem.* **2005**, *178*, 2042–2049. [CrossRef]
31. Taranu, B.-O.; Vlazan, P.; Svera, P.; Poienar, M.; Sfirloaga, P. New functional hybrid materials based on clay minerals for enhanced electrocatalytic activity. *J. Alloys Compd.* **2022**, *892*, 162239. [CrossRef]
32. Gao, F.; Lewis, R.A.; Wang, X.L.; Dou, S.X. Infrared absorption of lanthanum manganites. *Phys. C. Supercond. Appl.* **2000**, *341*, 2235–2236. [CrossRef]
33. Afify, M.S.; El Faham, M.M.; Eldemerdash, U.; El Rouby, W.M.A.; El-Dek, S.I. Room temperature ferromagnetism in Ag doped $LaMnO_3$ nanoparticles. *J. Alloys Compd.* **2021**, *861*, 158570. [CrossRef]
34. Ansari, A.A.; Ahmad, N.; Alam, M.; Adil, S.; Shahid, F.; Ramay, M.; Albadri, A.; Ahmad, A.; Al-Enizi, A.M.; Alrayes, B.F.; et al. Physico-chemical properties and catalytic activity of the sol-gel prepared Ce-ion doped $LaMnO_3$ perovskites. *Sci. Rep.* **2019**, *9*, 7747. [CrossRef] [PubMed]
35. Silverstein, R.M.; Bassler, G.C.; Morrill, T.C. *Spectrometric Identification of Organic Compounds*, 4th ed.; John Wiley and Sons: New York, NY, USA, 1981.
36. Aal, A.A.; Hammad, T.R.; Zawrah, M.; Battisha, I.K.; Abou Hammad, A.B. FTIR study of nanostructure perovskite $BaTiO_3$ doped with both Fe^{3+} and Ni^{2+} ions prepared by sol-gel technique. *Acta Phys. Pol. A* **2014**, *126*, 1318–1322.
37. Del Nero, J.; de Araujo, R.E.; Gomes, A.S.L.; de Melo, C.P. Theoretical and experimental investigation of the second hyperpolarizabilities of methyl orange. *J. Chem. Phys.* **2005**, *122*, 104506. [CrossRef]

38. Elumalai, S.; Muthuraman, G. Recovery of Methyl Orange and Congo Red from aqueous solutions using tri-octyl amine (TOA) in benzene as carrier. *Process Saf. Environ. Prot.* **2015**, *96*, 177–183. [CrossRef]
39. Rahman, M.; Pinky, T.A.; Mondal, D.C.; Abedin, M.; Hasan, M. The Study of the Photocatalytic Degradation of Methyl Orange in the Presence of Zinc Oxide (ZnO) Suspension. *J. Mater. Sci. Res. Rev.* **2020**, *5*, 1–14.
40. Youssef, N.A.; Shaban, S.A.; Ibrahim, F.A.; Mahmoud, A.S. Degradation of methyl orange using Fenton catalytic reaction. *Egypt. J. Pet.* **2016**, *25*, 317–321. [CrossRef]
41. Bala, S.S.; Alkhatib, A.J.; Bashir, S.S.; Abdulhadi, M. Photocatalytic Degradation of Indigo Carmine in Aqueous Solutions by the Antibacterial Agent Pefloxacin and UVA. *Biomed. J. Sci. Tech. Res.* **2018**, *5*, 4903–4909.
42. Olajire, A.A.; Olajide, A.J. Kinetic Study of Decolorization of Methylene Blue with Sodium Sulphite in Aqueous Media: Influence of Transition Metal Ions. *J. Phys. Chem. Biophys.* **2014**, *4*, 2.
43. Coates, E. Aggregation of Dyes in Aqueous Solutions. *J. Soc. Dye. Colour.* **1969**, *85*, 355–368. [CrossRef]
44. Barresi, A.A.; Mazza, D.; Ronchetti, S.; Spinicci, R.; Vallino, M. Non-stoichiometry and catalytic activity in ABO_3 perovskites: $LaMnO_3$ and $LaFeO_3$. *Stud. Surf. Sci. Catal.* **2000**, *130*, 1223–1228.
45. Ajmal, A.; Majeed, I.; Malik, R.N.; Idriss, H.; Nadeem, M. A Principles and mechanisms of photocatalytic dye degradation on TiO_2 based photocatalysts: A comparative overview. *RSC Adv.* **2014**, *4*, 37003–37026. [CrossRef]
46. Lin, X.; Huang, F.; Wang, W.; Shan, Z.; Shi, J. Methyl orange degradation over a novel Bi-based photocatalyst Bi_3SbO_7: Correlation of crystal structure to photocatalytic activity. *Dye. Pigment.* **2008**, *78*, 39–47. [CrossRef]
47. Ghiasi, M.; Malekzadeh, A. Solar photocatalytic degradation of methyl orange over $La_{0.7}Sr_{0.3}MnO_3$ nano-perovskite. *Sep. Purif. Technol.* **2014**, *134*, 12–19. [CrossRef]
48. Guo, J.; Chen, X.; Shi, Y.; Lan, Y.; Qin, C. Rapid Photodegradation of Methyl Orange (MO) Assisted with Cu(II) and Tartaric Acid. *PLoS ONE* **2015**, *10*, e0134298. [CrossRef]
49. Verduzco, L.E.; Garcia-Díaz, R.; Martinez, A.I.; Almanza Salgado, R.; Mendez-Arriaga, F.; Lozano-Morales, S.A.; Avendano-Alejo, M.; Padmasree, K.P. Degradation efficiency of methyl orange dye by $La_{0.5}Sr_{0.5}CoO_3$ perovskite oxide under dark and UV irradiated conditions. *Dye. Pigment.* **2020**, *183*, 108743. [CrossRef]
50. Naikwade, A.G.; Jagadale, M.B.; Kale, D.P.; Gophane, A.D.; Garadkar, K.M.; and Rashinkar, G.S. Photocatalytic Degradation of Methyl Orange by Magnetically Retrievable Supported Ionic Liquid Phase Photocatalyst. *ACS Omega* **2020**, *5*, 131–144.
51. Huang, H.; Sun, G.; Hu, J.; Jiao, T. Single-Step Synthesis of $LaMnO_3$/MWCNT Nanocomposites and Their Photocatalytic Activities. *Nanomater. Nanotechnol.* **2014**, *4*, 27. [CrossRef]
52. Zhong, W.; Jiang, T.; Dang, Y.; He, J.; Chen, S.-Y.; Kuo, C.-H.; Kriz, D.; Meng, Y.; Meguerdichian, A.; Sui, S.L. Mechanism studies on methyl orange dye degradation by perovskite-type $LaNiO_{3-\delta}$ under dark ambient conditions. *Appl. Catal. A Gen.* **2018**, *549*, 302–309. [CrossRef]